A Novel Perspective for Multi-modal Multi-label Skin Lesion Classification

Yuan Zhang[1]*, Yutong Xie[1], Hu Wang[2], Jodie C Avery[1], M Louise Hull[1], Gustavo Carneiro[3]

[1] University of Adelaide, Australia
[2] Mohamed bin Zayed University of Artificial Intelligence, United Arab Emirates
[3] University of Surrey, UK

Abstract

*The efficacy of deep learning-based Computer-Aided Diagnosis (CAD) methods for skin diseases relies on analyzing multiple data modalities (i.e., clinical+dermoscopic images, and patient metadata) and addressing the challenges of multi-label classification. Current approaches tend to rely on limited multi-modal techniques and treat the multi-label problem as a multiple multi-class problem, overlooking issues related to imbalanced learning and multi-label correlation. This paper introduces the innovative **Skin** Lesion Classifier, utilizing a **M**ulti-modal **M**ulti-label Trans**Former**-based model (**SkinM2Former**). For multi-modal analysis, we introduce the Tri-Modal Cross-attention Transformer (TMCT) that fuses the three image and metadata modalities at various feature levels of a transformer encoder. For multi-label classification, we introduce a multi-head attention (MHA) module to learn multi-label correlations, complemented by an optimisation that handles multi-label and imbalanced learning problems. SkinM2Former achieves a mean average accuracy of 77.27% and a mean diagnostic accuracy of 77.85% on the public Derm7pt dataset, outperforming state-of-the-art (SOTA) methods.*

1. Introduction

Skin cancer is the most common type of cancer in many countries, with melanoma accounting for over 80% of skin cancer deaths [30]. The 5-year survival rate for patients with early-stage melanoma exceeds 99%, dropping to 35% upon distant organ metastasis, emphasizing the importance of early detection and timely treatment [19, 31]. Dermatologists employ clinical and dermoscopic images, along with patient metadata, for comprehensive pattern analysis during skin cancer diagnosis [23]. Specifically, clinical images, captured using a digital camera, provide a macro-

scopic view with details such as colour, geometry, and overall appearance [27]. In contrast, dermoscopic images are obtained through dermoscopy, offering a magnified microscopic view of the lesion that uncovers detailed subsurface structures [17]. Furthermore, patient metadata, including location, gender, and age, supplements this analysis by providing contextual information [22]. To simplify the diagnostic process, the 7-Point Checklist [2], based on seven criteria to derive a diagnostic label (8 classification labels in total), is widely used for the primary diagnosis of skin cancer [34].

The importance of early skin cancer detection has motivated the medical image analysis community to explore deep learning-based Computer-Aided Diagnosis (CAD) tools to assist dermatologists in delivering precise diagnoses. However, many skin cancer classification methods, predominantly single-modal (dermoscopic image) multi-class approaches [13], are tailored to the limited ISIC benchmark [1, 7, 8, 11] and are not equipped to analyze multi-modal data or predict the multi-label 7-Point Checklist. This limitation hinders their integration into the clinical workflow described earlier, diminishing the likelihood of acceptance by clinicians.

Limited research exists on the simultaneous fusion of three modalities in skin cancer classification. Notable methods include Kawahara et al.'s late fusion using two Inception-V3 networks [15] (Figure 1a), FusionM4Net [32] and TFormer [40] with a hybrid fusion of imaging modalities, followed by a late fusion of metadata (Figure 1b). A limitation of the methods above is that they do not simultaneously fuse the three modalities at multiple feature levels, potentially overlooking important correlations of image and metadata features at distinct hierarchical levels. Furthermore, existing methods address the multi-label 7-point checklist classification as multiple multi-class learning problems, introducing imbalanced learning and neglecting label correlations [2, 15, 32, 36, 40], as Figure 2 shows.

In this paper, we address the automatic skin lesion classification challenges of multi-modality and multi-labeling

---

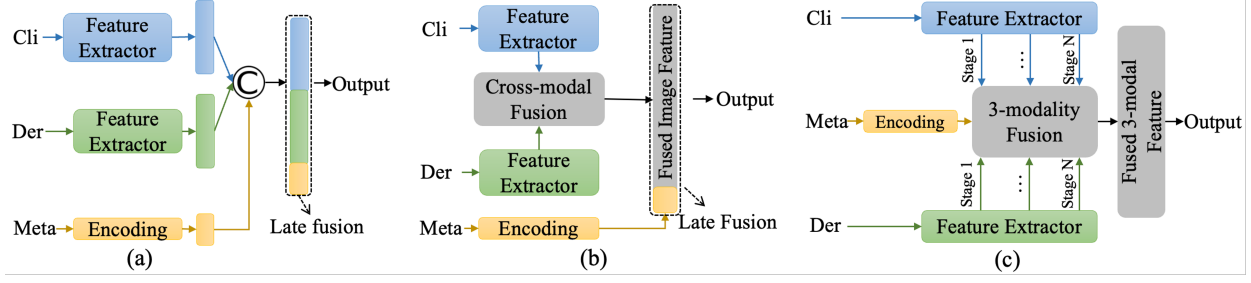*Corresponding author. Email: yuan.zhang01@adelaide.edu.au.

Figure 1. Multi-modal skin cancer classifier: (a) late fusion [15]; (b) hybrid fusion of image and late fusion of metadata [32, 40]; (c) our hybrid fusion of all modalities.
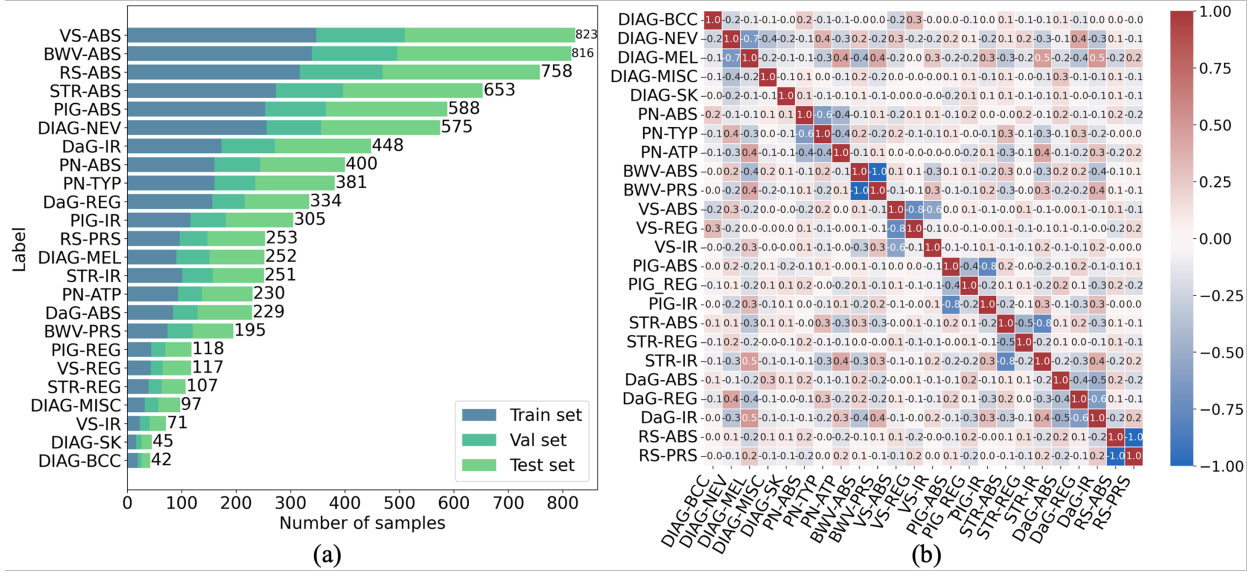

Figure 2. (a) Imbalanced distribution of samples per class. (b) Inter-label Pearson Correlation Coefficients heatmap. Note that labels are denoted by "Classification problem ({DIAG,PN,...})-Possible classes({ABS,NEV,...})".

through the introduction of the **Skin** Lesion Classifier built upon a **M**ulti-modal **M**ulti-label Trans**Former**-based model (**SkinM2Former**). The multi-modal challenge is addressed with a new Tri-Modal Cross-attention Transformer (TMCT) module to fuse dermoscopic image, clinical image, and metadata at multiple feature levels of a Swin transformer-based architecture [21], as Figure 1c shows. To handle the multi-label classification, we introduce a new attention mechanism to find label associations and a multi-label training [18] that is robust to imbalanced learning. Our contributions are:

- The new TMCT module to fuse multiple feature levels (from low to high level) of the three input data modalities (i.e., clinical image, dermoscopic image, and metadata).

- An innovative multi-label model comprising a new attention mechanism that learns the associations between different labels, and a multi-label training

strategy that is robust to imbalanced class distributions [18].

Experimental results on the public Derm7pt dataset demonstrate that our SkinM2Former achieves a mean accuracy of 77.27% and a mean diagnostic accuracy of 77.85%, which is significantly better than state-of-the-art (SOTA) methods.

2. Related Works

2.1. Automated Diagnosis of Skin Lesion

Computer-aided methods for classifying skin lesion images have drawn significant research attention because automated analysis can offer patients timely and consistent diagnoses, particularly in remote areas with limited access to clinical services. Previous research has primarily focused on utilizing a single dermoscopic modality. Bayasi et al. [3] propose Continual-GEN, a subnetwork-based sequential learning method for skin lesion classification that

2

trains with five datasets. Kanca et al. [14] develop a K-nearest neighbour algorithm that utilizes manually extracted features from the lesion areas on segmented dermoscopic images to classify melanoma, nevus, and seborrheic keratosis. Wang et al. [37] introduce a dual relational knowledge distillation framework SSD-KD to unify diverse knowledge for skin disease classification. However, these methods do not fully align with the standard diagnostic practices of dermatologists, which involve combining clinical images, dermoscopic images and patients' metadata to derive a comprehensive diagnosis. To bridge the gap, Derm7pt [15] was published as the first large-scale multi-modal and multi-label skin lesion classification dataset, thereby establishing a foundational framework for subsequent research in automated skin lesion classification.

2.2. Multi-modal Skin Lesion Classification

Multi-modal skin lesion classification research is becoming more prevalent. Patrício et al. [25] present CBE, a concept-based model for skin lesion diagnosis that integrates segmentation-based attention and coherence loss to enhance interpretability and classification accuracy. Bie et al. [5] propose a multi-level image-concept alignment framework MICA for explainable skin lesion classification, which combines a vision model with a language model and aligns the concept information with image semantic characteristics. However, these methods used only a subset of the Derm7pt dataset (827 images of Nevus and Melanoma), without focusing on the multi-label classification problem.

For methods focusing on the 7-Point Checklist, most employ a late fusion strategy to jointly analyse complementary information from different modalities. Kawahara et al. [15] propose the use of two Inception-V3 networks to extract clinical and dermoscopic image features that are concatenated with metadata in a late fusion approach. Tang et al. [32] present FusionM4Net, a multi-stage training approach that first extracts decision information using two CNN models from image modalities, then incorporates metadata at a later stage in the model. Alternatively, Zhang et al. [40] employ TFormer with a hybrid fusion strategy, initially fusing the two image modalities at the feature level and subsequently integrating metadata for classification also at a later stage of the model. However, these approaches do not concurrently integrate all three modalities at multiple feature levels, potentially missing significant correlations between image characteristics and metadata.

2.3. Multi-label Skin Lesion Classification with Imbalanced Learning

There is minimal focus on skin lesion classification from a multi-label perspective. The multi-label skin lesion classification in most previous studies has been handled by decomposing it into several independent multi-class

tasks [2, 15, 32, 36, 40], resulting in imbalance issues and ignoring label correlations. Effectively modelling label correlation and feature-label dependencies can reduce the complexity of learning processes and the dimension of the prediction space [6]. Wang et al. [35] utilise constrained classifier chain (CC) to enhance multi-label classification performance by minimizing binary cross-entropy (BCE) loss. However, CC requires each classifier to be binary, leading to the reassignment of originally multiple multi-class labels into a bunch of binary multi-labels, which compromises label precision.

Furthermore, the BCE loss introduces significant class imbalance issues. Mitigating these issues can prevent the model from overly emphasizing categories with more samples during training, thereby enhancing its generalization ability in real clinical scenarios [18, 33]. Previous research tackled the imbalance issue associated with BCE by employing simple methods such as frequency-based weighting [26] and adaptive weighting schemes [20, 28]. Therefore, exploring label correlations and utilizing advanced loss functions that bypass imbalance issues while enhancing discriminativity could serve as fundamental steps in studying skin classification from a multi-label perspective.

3. Methodology

The proposed SkinM2Former (Figure 3) has three components: a Tri-Modal Cross-attention Transformer (TMCT) to integrate the information from clinical images, dermoscopic images, and metadata at multiple feature levels; a Multi-Head Attention (MHA) module to capture correlations between labels; and a multi-label training method that is robust to class-distribution imbalances.

Let us represent the multi-modal skin-cancer dataset as $\mathcal{D} = \{(\mathbf{x}_i^{cli}, \mathbf{x}_i^{der}, \mathbf{x}_i^{meta}, \mathbf{y}_i)\}_{i=1}^N$ (e.g., Derm7t dataset [15]), with N clinical images $\mathbf{x}^{cli} \in \mathcal{X}^{cli} \subset \mathbb{R}^{W \times H \times C}$ (W, H and C are height, width and channels), dermoscopic images $\mathbf{x}^{der} \in \mathcal{X}^{der} \subset \mathbb{R}^{W \times H \times C}$ and metadata $\mathbf{x}^{meta} \in \mathcal{X}^{meta} \subset \mathbb{R}^L$ (L is the amount of metadata covariates), annotated with a set of multi-class labels $\mathbf{y}_i = \{(\mathbf{y}_i^{DIAG}, \mathbf{y}_i^{BWV}, \mathbf{y}_i^{PN}, \mathbf{y}_i^{VS}, \mathbf{y}_i^{RS}, \mathbf{y}_i^{STR}, \mathbf{y}_i^{DaG}, \mathbf{y}_i^{PIG})\}_{i=1}^N$. The labels in $\mathbf{y}_i$ represent one diagnosis label $\mathbf{y}^{DIAG} \in \{0,1\}^5$, and seven skin lesion attribute labels for each sample, where $\mathbf{y}^{BWV} \in \{0,1\}^2$, $\mathbf{y}^{PN} \in \{0,1\}^3$, $\mathbf{y}^{VS} \in \{0,1\}^3$, $\mathbf{y}^{RS} \in \{0,1\}^2$, $\mathbf{y}^{STR} \in \{0,1\}^3$, $\mathbf{y}^{DaG} \in \{0,1\}^3$, and $\mathbf{y}^{PIG} \in \{0,1\}^3$.

3.1. Tri-Modal Cross-modality Fusion

The proposed TMCT module (Figure 3) integrates multi-scale clinical and dermoscopic image features (leveraging Swin Transformer [21] for its effective long-range dependency capture [12]) with metadata features from a multi-layer perceptron (MLP). In the first TMCT module, clin-
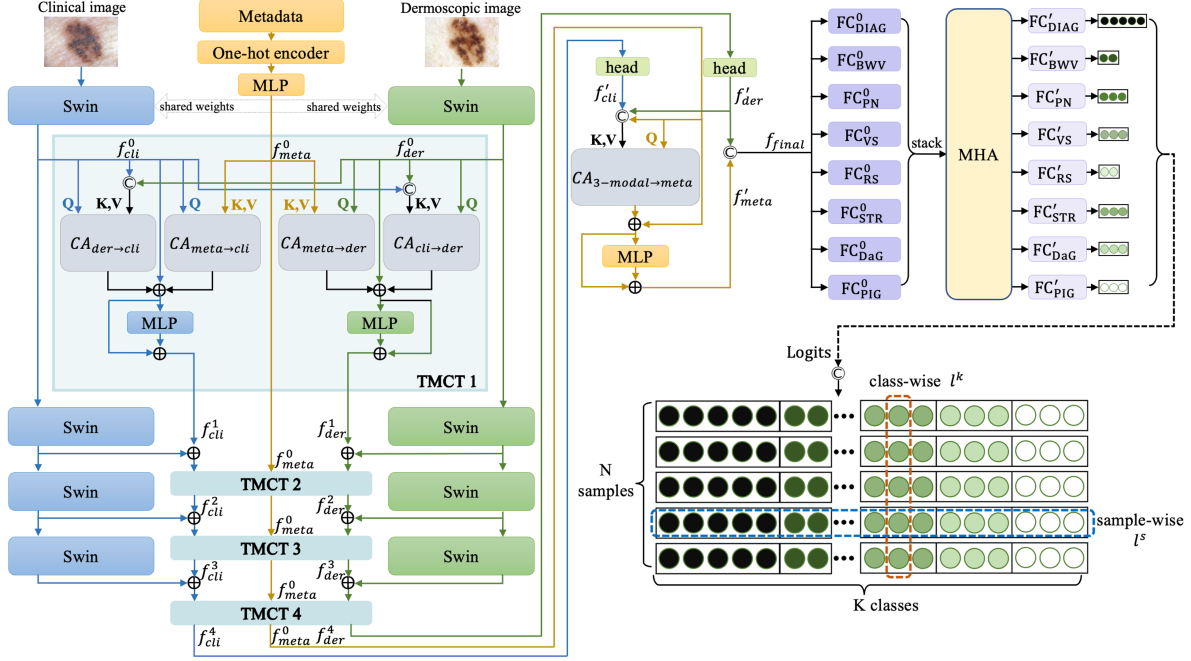
Figure 3. **SkinM2Former**: Tri-modal Cross-attention Transformer (TMCT) module to fuse all modalities; multi-head attention (MHA) layer to learn multi-label associations; and multi-label loss [18] robust to class imbalances.

ical image features f_{cli}^0 and dermoscopic image features f_{der}^0 from the first Swin Transformer block, alongside metadata feature f_{meta}^0, are fused using cross-modal attention (CA) blocks. The details of $CA_{der \to cli}$ & $CA_{meta \to cli}$ and $CA_{cli \to der}$ & $CA_{meta \to der}$ are the same, so we only describe $CA_{der \to cli}$, $CA_{meta \to cli}$. The $CA_{der \to cli}$ uses f_{cli}^0 as the query and the concatenation of f_{cli}^0 and f_{der}^0 (denoted by $[f_{cli}^0, f_{der}^0]$) as the key and value [40]; and for $CA_{meta \to cli}$, we apply a multi-head attention layer which takes f_{cli}^0 as the query and f_{meta}^0 as the key and value, calculated as

$$CA_{der \to cli} = \text{window\_multihead}(f_{cli}^0, f_{der}^0), \quad (1)$$

$$CA_{meta \to cli} = \text{multihead}(f_{cli}^0, f_{meta}^0). \quad (2)$$

The output of $CA_{der \to cli}$ and $CA_{meta \to cli}$ are combined and connected with the initial input f_{cli}^0 via a residual operation, then passed to an MLP with a residual shortcut. Finally, we have the new clinical image future f_{cli}^1 which integrates the information from both dermoscopic image and metadata as follows:

$$f_{cli}^1 = \text{MLP} \left(CA_{der \to cli} + CA_{meta \to cli} + f_{cli}^0 \right)$$
$$+ CA_{der \to cli} + CA_{meta \to cli} + f_{cli}^0. \quad (3)$$

The internal representations of the clinical image are refined through dual cross-attention blocks, effectively incorporating features from dermoscopic images and metadata. This synergistic fusion within a latent space enhances the

model's adaptability and utilization of complementary information across modalities. The same fusion strategy is applied to dermoscopic images to yield f_{der}^1. The outputs of the first TMCT module are f_{cli}^1, f_{der}^1, and a copy of f_{meta}^0. To improve the capability of capturing cross-modal information across varying scales, we combine the features extracted by each modality backbone to f_{cli}^1 and f_{der}^1 respectively, then compound with f_{meta}^0, as the input of the next TMCT module. We apply one TMCT module after each stage of the backbone, to gradually fuse the features from low to high level. After the fourth TMCT module, the output f_{cli}^4 and f_{der}^4 are fed into two head modules consisting of a pooling layer and a fully connected layer to get the final fused image feature vectors f_{cli}' and f_{der}'.

To enhance further the feature fusion between image and non-image modalities, we apply an attention-based transformer block $CA_{3-modal \to meta}$ which takes metadata feature f_{meta}^0 as query and the concatenation of f_{cli}', f_{der}', f_{meta}^0 as key and value, with $CA_{3-modal \to meta} = \text{multihead}\left(f_{meta}^0, [f_{cli}', f_{der}', f_{meta}^0]\right)$.

Then, we feed the output into an MLP with a residual shortcut to get the fused metadata feature f_{meta}' as follows:

$$f_{meta}' = \text{MLP} \left(\text{multihead} \left(f_{meta}^0, [f_{cli}', f_{der}', f_{meta}^0] \right) + f_{meta}^0 \right)$$
$$+ \text{multihead} \left(f_{meta}^0, [f_{cli}', f_{der}', f_{meta}^0] \right) + f_{meta}^0. \quad (4)$$

After this Tri-Modal cross-modality fusion, we get the feature f_{final} for the following classification module by

4

concatenating dermoscopic feature f'_{der} and the metadata feature f'_{meta} as follows:

$$f_{final} = [f'_{der}, f'_{meta}]. \qquad (5)$$

3.2. Multi-label Classification

We employ a Multi-Head Attention (MHA) layer to estimate the correlations among various attributes. Specifically, we pass the classification feature f_{final} into a set of 8 fully connected (FC) layers to get the initial classification features for each attribute. These features are stacked and passed to the MHA. The output from the MHA is subsequently unstacked and input into another set of 8 classification layers to yield the multi-label probabilities $\mathbf{p}_i = \{(\mathbf{p}_i^{DIAG}, \mathbf{p}_i^{PN}, \mathbf{p}_i^{BWV}, \mathbf{p}_i^{VS}, \mathbf{p}_i^{PIG}, \mathbf{p}_i^{STR}, \mathbf{p}_i^{DaG}, \mathbf{p}_i^{RS})\}_{i=1}^N$ for the diagnosis of skin diseases. Assuming that the logit vectors to produce these probabilities are represented by $\mathbf{l}_i = \{(\mathbf{l}_i^{DIAG}, \mathbf{l}_i^{PN}, \mathbf{l}_i^{BWV}, \mathbf{l}_i^{VS}, \mathbf{l}_i^{PIG}, \mathbf{l}_i^{STR}, \mathbf{l}_i^{DaG}, \mathbf{l}_i^{RS})\}_{i=1}^N$, we train our model with the Two-Way Loss function (TWL), that is shown to be robust to the class imbalances present in multi-label learning [18]:

$$\ell = \frac{1}{N}\sum_{i=1}^{N} \ell_{sp}(\{(\mathbf{l}_{ik}, \mathbf{y}_{ik})\}_{k=1}^{K}; T) + \frac{1}{K}\sum_{k=1}^{K} \ell_{sp}(\{(\mathbf{l}_{ik}, \mathbf{y}_{ik})\}_{i=1}^{N}; T), \qquad (6)$$

which is optimised over the N samples and K labels using

$$\ell_{sp}(\{(\mathbf{l}_{ik}, \mathbf{y}_{ik})\}_{k=1}^{K}; T) =$$
$$\mathsf{softplus}\left(\log \sum_{n=1|y_{in}=0}^{K} e^{\mathbf{l}_{in}} + T \log \sum_{p=1|y_{ip}=1}^{K} e^{-\frac{\mathbf{l}_{ip}}{T}}\right), \qquad (7)$$

and $\ell_{sp}(\{(\mathbf{l}_{ik}, \mathbf{y}_{ik})\}_{i=1}^{N}; T) =$
$$\mathsf{softplus}\left(\log \sum_{i=1|\mathbf{y}_{ik}=0}^{N} e^{\mathbf{l}_{ik}} + T \log \sum_{j=1|\mathbf{y}_{jk}=1}^{N} e^{-\frac{\mathbf{l}_{jc}}{T}}\right). \qquad (8)$$

This TWL function addresses class imbalance in multi-label learning by discriminating both classes and samples, which mitigates the imbalance problem more effectively than traditional BCE loss [18].

During the evaluation, we compute $\mathbf{p}$, where the label for each of the 8 attributes is computed as the one with maximum probability.

4. Experiments

4.1. Dataset and Implementation Details

We evaluate our SkinM2Former on the Derm7pt dataset [15], which is the main medical dataset for the multi-modal, multi-label, imbalanced learning task. It containing 1011 cases, each comprising a dermoscopic image, a clinical image, patient's metadata, and 8 labels (7-point checklist labels and a diagnosis label). The 7-point checklist

Table 1. The detailed statistics for the Derm7pt dataset.

Label	Name	Abbrev	Train	Val	Test	Total
DIAG	Basal Cell Carcinoma	BCC	19	7	16	42
	Nevus	NEV	256	100	219	575
	Melanoma	MEL	90	61	101	252
	Miscellaneous	MISC	32	25	40	97
	Seborrheic Keratosis	SK	16	10	19	45
BWV	Absent	ABS	339	157	320	816
	Present	PRS	74	46	75	195
PN	Absent	ABS	160	84	156	400
	Typical	TYP	160	75	146	381
	Atypical	ATP	93	44	93	230
VS	Absent	ABS	347	163	313	823
	Regular	REG	43	22	52	117
	Irregular	IR	23	18	39	71
RS	Absent	ABS	317	152	289	758
	Present	PRS	96	51	106	253
STR	Absent	ABS	273	123	257	653
	Regular	REG	39	24	44	107
	Irregular	IR	101	56	94	251
DaG	Absent	ABS	84	45	100	229
	Regular	REG	156	60	118	334
	Irregular	IR	173	98	177	448
PIG	Absent	ABS	253	112	223	588
	Regular	REG	44	26	48	118
	Irregular	IR	226	65	124	305

labels include: blue whitish veil (BWV), pigment network (PN), vascular structures (VS), regression structures (RS), streaks (STR), dots and globules (DaG), and pigmentation (PIG). Each label has different types, including: Present (PRE), Absent (ASB), Typical (TYP), Atypical (ATP), Regular (REG), and Irregular (IR). The diagnosis (DIAG) label is divided into five types: Basal Cell Carcinoma (BCC), Nevus (NEV), Melanoma (MEL), Miscellaneous (MISC), and Seborrheic Keratosis (SK). More details of the dataset are in [15]. These 1011 cases are split into 413 training, 203 validation and 395 testing cases by [15]. Table 1 lists details of dataset distribution.

Our model was trained for 200 epochs with a batch size of 32, using Adam optimizer [16] with an initial learning rate of 1e-4 and a weight decay of 1e-4. The CosineAnnealingLR schedule is applied for the learning rate decay. The model with the best average accuracy on the validation set is saved for testing. The ImageNet-1K [29] pre-trained Swin-Tiny is employed as the backbone. The dimension of both heads, all MLPs, and all FC layers is 128. The number of heads of MHA is 4. The temperature parameter $T = 4$. Input images are resized to $224 \times 224 \times 3$, and the length of the encoded patient's meta-data is 20. Data augmentation consists of random vertical and horizontal flips, shifts, distortions and mixup [9]. All experiments were performed using Python 3.9 with PyTorch 1.12.1 and run on 4 NVIDIA

RTX 3090 GPUs with 24 GB VRAM.

Following [4, 15], our approach is evaluated with the average accuracy (AVG) of all classes. We also show F1-score results in Table 2 of the supplementary material since this is a valuable comparison measure, but not as common as AVG. All experiments are run 10 times, from which we report the mean and standard deviation values.

4.2. Experimental Results

4.2.1 Comparisons with SOTA

We compare the performance of our method to the following SOTA methods: Inception-unbalanced (Inception_UB), Inception-balanced (Inception_B) and Inception-combine (Inception_CB) methods proposed by [15], MmA [24], TripleNet [10], EmbeddingNet [39], HcCNN [4], AM-FAM [36], FusionM4Net [32], and TFormer [40].

The results in Table 2 show that SkinM2Former achieves an average accuracy of 77.27%, representing a statistically significant improvement over the current leading methods, FusionM4Net and TFormer. The most competitive method in terms of average accuracy is the FusionM4Net, which requires multi-stage training and searching for decision weights for each classifier using the validation set. Such complex training is a clear disadvantage, compared to our proposed end-to-end training method.

Moreover, the results in Table 3 indicate that our method also achieved the highest F1-score on the majority of labels, which further displays the effectiveness of our method.

Table 4 illustrates the clinical images, dermoscopic images, and detailed patient metadata of 6 examples, along with their predicted labels generated by FusionM4Net [20], TFormer [25], and our proposed SkinM2Former. Comparing the predicted labels with the most competitive methods, FusionM4Net [32] and TFormer [40], reveals that our approach accurately predicts the majority of labels.

4.2.2 Ablation study

To validate the efficacy of each component in SkinM2Former, we conducted the ablation study in Table 5. Our baseline model uses a shared weights (SW) Swin-Tiny (Swin) as the feature extractor for imaging modalities, employing concatenation as the feature fusion strategy and Binary Cross-Entropy (BCE) as the loss function. Note that the TMCT module enhances feature extraction and fusion across the three modalities, where the average accuracy increases from 74.92% to 75.92%. For the multi-label classification strategies (MHA and TWL), we notice that TMTC+TWL, in comparison with TMTC+BCE, shows a small, but consistent gain of 0.22%. The addition of MHA forms TMTC+MHA+TWL (SkinM2Former), which when compared to TMTC+MHA+BCE, shows a substantial improvement of 1.24%. Furthermore,

TMTC+MHA+TWL, in comparison with TMTC+TWL, shows a remarkable improvement of 1.13%. It is worth noticing that TMTC+MHA+TWL improved the average accuracy of the baseline from 74.92% to 77.27%. These results support our claims about the TMCT (fusion of multiple feature levels), MHA (interrelations among labels) and TWL (multi-label learning).

Moreover, the results from the third-to-last row of Table 5 indicate that, within the TMCT module, utilizing f^0_{meta} directly as key and value in $CA_{meta \to cli}$ and $CA_{meta \to der}$ leads to higher classification accuracy compared to using the concatenation of f^0_{meta} and image modalities. Therefore, we employ f^0_{meta} as the key and value for $CA_{meta \to cli}$ and $CA_{meta \to der}$ in all experiments. Additionally, comparing the results between the last and the second-to-last rows of Table 5, we see that using independent feature extractors for two image modalities led to a 0.83% decrease in average accuracy, demonstrating the effectiveness of Swin Transformers with shared weights across different modalities. Conclusively, using shared weights in feature extractors not only reduces the number of parameters but also enhances the ability to capture and integrate features from both dermoscopic and clinical images.

4.2.3 Analysis for multi-modality feature fusion

We compare the use of unimodal and multi-modal data in Table 6. Unimodal results for each modality show relatively low accuracy across different labels, with dermoscopic images outperforming metadata, which surpasses clinical images. The multi-modal data results suggest that the fusion of two or three modalities enhances accuracy, revealing that diverse modalities contain complementary information that are advantageous for classification. In fact, our proposed fusion of the three modalities at multiple feature levels produces the best classification accuracy of 77.27%.

4.2.4 Analysis for multi-modality decision fusion

Table 7 shows a comparison of different concatenations of decision features from distinct modalities (f'_{cli}, f'_{der} and f'_{meta}) to build the final decision feature f_{final}. Results show that SkinM2Former reaches the highest accuracy of 77.27% when concatenating f'_{der} and f'_{meta} to form f_{final}. Even though the best DIAG accuracy of 78.25% is achieved by concatenating f'_{cli}, f'_{der} and f'_{meta}, such concatenation of the three decision features only reaches an average of 76.82%. This can be explained by the presence of excessive noise in clinical images. However, this does not imply that clinical images are dispensable because their contribution may have been implicitly passed to the model through the TMCT module. Given these results, our SkinM2Former relies on the concatenation of f'_{cli} and f'_{der} to build the f_{final}.

6

Table 2. Comparisons against SOTA methods (test accuracy %). We only compare methods using the officially published Derm7t dataset train/validation/test split. Due to TFomer not specifying the number of experiment runs, for a fair comparison, we reproduce their results using the provided code and parameters, reporting the averages from 10 runs. The remaining results are all obtained from papers [4,32,36]. The p-value (last column) is calculated from the AVG result by one-tailed paired t-tests between each method against SkinM2Former.

Method	DIAG	BWV	PN	VS	RS	STR	DaG	PIG	**AVG**	p-value
Inception_UB	68.4	87.6	68.1	81.3	78.2	75.9	56.7	65.6	72.7	0.0045
Inception_B	70.8	87.3	68.9	81.5	78.2	75.7	60.3	64.8	73.4	0.0023
Inception_CB	74.2	87.1	70.9	79.7	77.2	74.2	60.0	66.1	73.7	0.0002
MmA	70.6	83	65.6	75.7	73.9	69.4	59.2	61.3	69.8	8.5×10^{-7}
EmbeddingNet	68.6	84.3	65.1	82.5	78.0	73.4	57.5	64.3	71.7	0.0011
TripleNet	68.6	87.9	63.3	83.0	76.0	74.4	61.3	67.3	72.7	0.0058
HcCNN	69.9	87.1	70.6	**84.8**	80.8	71.6	65.6	68.6	74.9	0.0310
AMFAM	75.4	88.1	70.6	83.3	80.8	74.7	63.8	70.9	76.0	0.0075
FusionM4Net	77.6±1.5	88.5±0.4	69.2±1.5	81.6±0.5	**81.4±0.8**	76.1±1.1	64.4±0.7	71.3±1.3	76.3±0.7	0.0490
TFormer	77.5±0.2	87.1±0.1	72.4±0.1	82.1±0.1	80.7±0.1	75.4±0.1	65.5±0.2	68.5±0.2	76.2±0.5	0.0096
SkinM2Former	**77.85±0.09**	**88.83±0.09**	**73.67±0.20**	82.75±0.10	81.23±0.06	**76.11±0.15**	65.82±0.09	71.93±0.10	**77.27±0.47**	NA

Table 3. Comparisons of top-performing SOTA methods (F1-score). The F1 score is calculated as the harmonic mean of the precision and recall scores. We only compare methods using the official Derm7t dataset with fixed train, validation, and test sets. TFormer results are replicated using their code and parameters, with averages from 10 experiments reported. The HcCNN did not give detailed results [4]. The rest of the results are all obtained from papers [32,38,40].

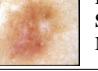| Method	DIAG	BWV	PN	VS	RS	STR	DaG	PIG	**AVG**
Inception-UB	43.92	76.39	63.88	**61.23**	64.96	60.15	53.77	48.04	59.04
Inception-B	50.25	73.62	65.64	47.10	64.88	63.98	58.37	53.00	59.60
Inception-CB	63.40	80.63	68.31	50.62	72.40	63.33	58.60	56.26	64.19
AMFAM	55.02	79.08	68.42	48.45	73.38	65.32	61.54	62.26	64.18
FusionM4Net	57.70	80.58	68.67	42.88	72.26	67.35	63.34	56.64	63.68
Tformer	66.86	78.88	71.15	57.04	73.87	66.00	63.09	61.82	67.34
SkinM2Former	**66.88**	**81.22**	**72.15**	56.57	**74.41**	**67.38**	63.62	**64.85**	**68.38**

Table 4. Examples of clinical image, dermoscopic image, and patient metadata, along with the predicted labels from FusionM4Net [32], TFormer [40], and our SkinM2Former. Ground truth (GT) is in the second column of the tables.

Diagnostic Difficulty: high
Elevation: palpable
Location: upper limbs
Sex: female
Management: excision

Label	GT	FusionM4Net	TFormer	SkinM2Former
DIAG	BCC	NEV	BCC	BCC
PN	ABS	ABS	ABS	ABS
BWV	ABS	ABS	ABS	ABS
VS	ABS	ABS	IR	ABS
PIG	ABS	ABS	IR	ABS
STR	ABS	ABS	ABS	ABS
DaG	IRG	IRG	IRG	IRG
RS	ABS	ABS	ABS	ABS

Diagnostic Difficulty: medium
Elevation: flat
Location: buttocks
Sex: male
Management: excision

Label	GT	FusionM4Net	TFormer	SkinM2Former
DIAG	NEV	NEV	NEV	NEV
PN	TYP	ATP	ATP	TYP
BWV	ABS	ABS	ABS	ABS
VS	ABS	ABS	ABS	ABS
PIG	ABS	ABS	ABS	ABS
STR	IR	ABS	ABS	IR
DaG	IRG	REG	IRG	IRG
RS	ABS	ABS	ABS	ABS

Diagnostic Difficulty: medium
Elevation: nodular
Location: lower limbs
Sex: female
Management: excision

Label	GT	FusionM4Net	TFormer	SkinM2Former
DIAG	MEL	MEL	MEL	MEL
PN	ABS	ABS	ATP	ABS
BWV	PRS	ABS	ABS	PRS
VS	IR	ABS	IR	IR
PIG	IR	ABS	IR	IR
STR	IR	ABS	IR	IR
DaG	IRG	ABS	IRG	IRG
RS	ABS	ABS	ABS	ABS

Diagnostic Difficulty: high
Elevation: palpable
Location: chest
Sex: female
Management: excision

Label	GT	FusionM4Net	TFormer	SkinM2Former
DIAG	MEL	MEL	MEL	MEL
PN	ATP	ABS	ATP	ATP
BWV	ABS	ABS	ABS	ABS
VS	ABS	ABS	ABS	ABS
PIG	IR	IR	IR	IR
STR	IR	IR	IR	IR
DaG	REG	IRG	IRG	IRG
RS	ABS	ABS	ABS	ABS

Diagnostic Difficulty: medium
Elevation: palpable
Location: back
Sex: male
Management: clinical follow up

Label	GT	FusionM4Net	TFormer	SkinM2Former
DIAG	MISC	BCC	MISC	MISC
PN	TYP	TYP	TYP	TYP
BWV	ABS	ABS	ABS	ABS
VS	ABS	ABS	ABS	ABS
PIG	ABS	ABS	IR	ABS
STR	ABS	ABS	ABS	ABS
DaG	IRG	REG	IRG	IRG
RS	ABS	ABS	REG	ABS
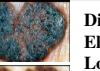
Diagnostic Difficulty: low
Elevation: palpable
Location: back
Sex: male
Management: no further examination

Label	GT	FusionM4Net	TFormer	SkinM2Former
DIAG	SK	MEL	SK	SK
PN	ABS	ABS	TYP	ABS
BWV	ABS	PRS	ABS	ABS
VS	ABS	ABS	ABS	ABS
PIG	IR	IR	IR	IR
STR	ABS	ABS	ABS	ABS
DaG	ABS	IRG	IRG	IRG
RS	ABS	ABS	ABS	ABS

Table 5. The ablation study results of our SkinM2Former (test accuracy %).

Method	SW	DIAG	BWV	PN	VS	RS	STR	DAG	PIG	**AVG**
Swin+BCE (Baseline)	●	72.81±0.24	88.20±0.05	68.86±0.13	82.48±0.05	78.78±0.10	74.03±0.24	62.99±0.12	71.19±0.12	74.92±0.79
TMCT+BCE	●	76.38±0.14	87.75±0.07	71.72±0.22	82.25±0.07	80.02±0.11	76.15±0.18	64.78±0.21	68.28±0.15	75.92±0.70
TMCT+TWL	●	76.00±0.15	87.92±0.10	71.52±0.16	82.28±0.15	80.18±0.10	76.08±0.20	65.77±0.16	69.39±0.26	76.14±0.61
TMCT+MHA+BCE	●	76.51±0.20	87.09±0.12	71.11±0.18	82.25±0.12	80.00±0.13	75.22±0.13	**66.78±0.13**	69.29±0.15	76.03±0.75
TMCT(concat.image)+MHA+TWL	●	77.75±0.10	**89.11±0.10**	72.48±0.10	82.46±0.11	80.15±0.12	75.27±0.19	65.49±0.12	71.34±0.20	76.76±0.39
TMCT+MHA+TWL	○	77.22±0.11	88.08±0.10	72.18±0.13	82.41±0.10	79.70±0.17	75.04±0.14	64.71±0.16	**72.23±0.15**	76.44±0.68
TMCT+MHA+TWL(Ours)	●	**77.85±0.09**	88.83±0.09	**73.67±0.20**	82.75±0.10	**81.23±0.06**	**76.11±0.15**	65.82±0.09	71.93±0.10	**77.27±0.47**

Table 6. Single vs. multi-modal skin lesion classification (test accuracy %).

Modality	DIAG	BWV	PN	VS	RS	STR	DAG	PIG	**AVG**
Cli	62.23±0.06	84.81±0.10	57.87±0.20	**84.81±0.10**	74.78±0.14	65.32±0.15	54.70±0.18	61.01±0.14	67.62±0.69
Der	71.75±0.16	88.21±0.06	66.58±0.14	81.57±0.07	79.59±0.12	75.80±0.10	60.76±0.04	70.08±0.17	74.29±0.39
Meta	71.90±0.21	85.16±0.03	59.44±0.07	79.14±0.01	72.76±0.05	71.75±0.08	59.70±0.05	59.65±0.04	69.94±0.43
Cli+Der	73.13±0.14	87.49±0.10	69.77±0.11	83.59±0.09	80.66±0.08	74.84±0.19	63.09±0.09	68.15±0.25	75.09±0.54
Cli+Meta	71.80±0.16	85.67±0.05	63.80±0.11	80.66±0.17	75.54±0.14	69.82±0.18	60.10±0.16	61.32±0.32	71.09±0.60
Der+Meta	77.32±0.06	88.56±0.09	73.06±0.18	81.32±0.09	79.44±0.07	**76.71±0.26**	65.67±0.19	71.65±0.08	76.72±0.42
Cli+Der+Meta	**77.85±0.09**	**88.83±0.09**	**73.67±0.20**	82.75±0.10	**81.23±0.06**	76.11±0.15	**65.82±0.09**	**71.93±0.10**	**77.27±0.47**

Table 7. Classification (test accuracy %) using a final feature f_{final} obtained by concatenating different decision features (f'_{cli}, f'_{der} and f'_{meta}).

Modality	DIAG	BWV	PN	VS	RS	STR	DAG	PIG	**AVG**
f'_{cli}	72.71±0.11	87.49±0.14	70.76±0.17	82.73±0.10	79.97±0.10	74.59±0.19	62.05±0.14	69.75±0.16	74.88±0.53
f'_{der}	72.51±0.21	88.00±0.08	70.86±0.15	82.46±0.09	79.75±0.13	75.37±0.16	63.62±0.20	71.01±0.17	75.45±0.55
f'_{meta}	76.38±0.09	88.84±0.04	66.91±0.02	80.51±0.11	77.75±0.06	72.78±0.13	63.49±0.13	68.89±0.16	74.43±0.49
$f'_{cli}+f'_{der}$	72.05±0.11	87.92±0.08	70.03±0.11	**83.39±0.10**	79.44±0.17	74.68±0.12	62.46±0.14	69.37±0.21	74.92±0.64
$f'_{cli}+f'_{meta}$	77.42±0.11	**89.01±0.07**	72.03±0.15	83.22±0.09	80.58±0.16	73.95±0.17	64.61±0.11	69.77±0.15	76.32±0.67
$f'_{der}+f'_{meta}$	77.85±0.09	88.83±0.09	**73.67±0.20**	82.75±0.10	**81.23±0.06**	76.11±0.15	65.82±0.09	71.93±0.10	77.27±0.47
$f'_{cli}+f'_{der}+f'_{meta}$	**78.25±0.12**	88.51±0.06	72.61±0.09	83.06±0.09	80.51±0.12	75.54±0.18	65.11±0.14	70.99±0.15	76.82±0.33

4.3. Analysis of Model Applicability in Real-world Scenarios

Our proposed method is highly applicable in real-world clinical settings. SkinM2Former has been carefully designed, with each component tailored to address challenges associated with multi-modal, multi-label tasks, and class imbalance issues. Table 5 demonstrated the effectiveness and importance of these components. Moreover, training our model requires approximately 1 hour, a process that occurs offline. Once trained, the model classifies each sample in less than 0.03 seconds. This speed suggests that our approach is well-suited for integration into routine clinical workflows.

5. Limitations

Our approach did not consider the presence of potential confounding variables on the images, such as grid scales and hair, which may have an impact on model performance. Future research could leverage methods to detect and remove confounding factors [38]. Furthermore, a hierarchical relationship exists between 8 main labels and 24 specific labels, which our research did not specifically address. Future studies could utilize Graph Convolutional Networks (GCN) to better capture this hierarchical relationship, thereby enhancing the model's classification capabilities.

6. Conclusion

In this work, we introduced SkinM2Former for multi-modal multi-label classification of skin lesions. We designed a set of TMCT modules to progressively fuse cross-modal information between three modalities at the feature level. Moreover, we formulated the classification problem of skin lesions from a multi-label perspective, proposing to enhance classification performance by exploring label dependencies and employing more effective loss functions. Experimental results on the publicly available Derm7pt multi-modal multi-label dataset demonstrate that our approach outperforms other SOTA methods. In addition, we hope our research offers insights for the automated detection of other diseases requiring multi-modal multi-label diagnostics. For instance, multifocal diseases like endometriosis require diagnoses of multiple lesions from various medical image modalities (e.g., MRI and ultrasound).

References

[1] Zawacki Anna, Helba Brian, Shih George, Weber Jochen, Elliott Julia, Combalia Marc, et al. Siim-isic melanoma classification, 2020. 1

[2] Giuseppe Argenziano, C Catricalà, M Ardigo, P Buccini, PASQUALINO De Simone, L Eibenschutz, et al. Seven-point checklist of dermoscopy revisited. British Journal of Dermatology, 164(4):785–790, 2011. 1, 3

[3] Nourhan Bayasi, Siyi Du, Ghassan Hamarneh, and Rafeef Garbi. Continual-gen: Continual group ensembling for domain-agnostic skin lesion classification. In International Conference on Medical Image Computing and Computer-Assisted Intervention, pages 3–13. Springer, 2023. 2

[4] Lei Bi, David Dagan Feng, Michael Fulham, and Jinman Kim. Multi-label classification of multi-modality skin lesion via hyper-connected convolutional neural network. Pattern Recognition, 107:107502, 2020. 6, 7

[5] Yequan Bie, Luyang Luo, and Hao Chen. Mica: Towards explainable skin lesion diagnosis via multi-level image-concept alignment. In Proceedings of the AAAI Conference on Artificial Intelligence, volume 38, pages 837–845, 2024. 3

[6] Xiaoya Che, Degang Chen, and Jusheng Mi. Label correlation in multi-label classification using local attribute reductions with fuzzy rough sets. Fuzzy Sets and Systems, 426:121–144, 2022. 3

[7] Noel Codella, Veronica Rotemberg, Philipp Tschandl, M Emre Celebi, Stephen Dusza, David Gutman, et al. Skin lesion analysis toward melanoma detection 2018: A challenge hosted by the international skin imaging collaboration (isic). arXiv preprint arXiv:1902.03368, 2019. 1

[8] Noel CF Codella, David Gutman, M Emre Celebi, Brian Helba, Michael A Marchetti, Stephen W Dusza, et al. Skin lesion analysis toward melanoma detection: A challenge at the 2017 international symposium on biomedical imaging (isbi), hosted by the international skin imaging collaboration (isic). In 2018 IEEE 15th international symposium on biomedical imaging (ISBI 2018), pages 168–172. IEEE, 2018. 1

[9] Justin Engelmann, Alice D McTrusty, Ian JC MacCormick, Emma Pead, Amos Storkey, and Miguel O Bernabeu. Detecting multiple retinal diseases in ultra-widefield fundus imaging and data-driven identification of informative regions with deep learning. Nature Machine Intelligence, 4(12):1143–1154, 2022. 5

[10] Zongyuan Ge, Sergey Demyanov, Rajib Chakravorty, Adrian Bowling, and Rahil Garnavi. Skin disease recognition using deep saliency features and multimodal learning of dermoscopy and clinical images. In Medical Image Computing and Computer Assisted Intervention- MICCAI 2017: 20th International Conference, Quebec City, QC, Canada, September 11-13, 2017, Proceedings, Part III 20, pages 250–258. Springer, 2017. 6

[11] David Gutman, Noel CF Codella, Emre Celebi, Brian Helba, Michael Marchetti, Nabin Mishra, et al. Skin lesion analysis toward melanoma detection: A challenge at the international symposium on biomedical imaging (isbi) 2016, hosted by the international skin imaging collaboration (isic). arXiv preprint arXiv:1605.01397, 2016. 1

[12] Kai Han, Yunhe Wang, Hanting Chen, Xinghao Chen, Jianyuan Guo, Zhenhua Liu, et al. A survey on vision transformer. IEEE transactions on pattern analysis and machine intelligence, 45(1):87–110, 2022. 3

[13] Md Kamrul Hasan, Md Asif Ahamad, Choon Hwai Yap, and Guang Yang. A survey, review, and future trends of skin lesion segmentation and classification. Computers in Biology and Medicine, page 106624, 2023. 1

[14] Elif Kanca and Selen Ayas. Learning hand-crafted features for k-nn based skin disease classification. In 2022 international congress on human-computer interaction, optimization and robotic applications (HORA), pages 1–4. IEEE, 2022. 3

[15] Jeremy Kawahara, Sara Daneshvar, Giuseppe Argenziano, and Ghassan Hamarneh. Seven-point checklist and skin lesion classification using multitask multimodal neural nets. IEEE journal of biomedical and health informatics, 23(2):538–546, 2018. 1, 2, 3, 5, 6

[16] Diederik P Kingma and Jimmy Ba. Adam: A method for stochastic optimization. arXiv preprint arXiv:1412.6980, 2014. 5

[17] Harald Kittler. Evolution of the clinical, dermoscopic and pathologic diagnosis of melanoma. Dermatology Practical & Conceptual, 11(Suppl 1), 2021. 1

[18] Takumi Kobayashi. Two-way multi-label loss. In Proceedings of the IEEE/CVF Conference on Computer Vision and Pattern Recognition, pages 7476–7485, 2023. 2, 3, 4, 5

[19] Ulrike Leiter, Ulrike Keim, and Claus Garbe. Epidemiology of skin cancer: update 2019. Sunlight, Vitamin D and Skin Cancer, pages 123–139, 2020. 1

[20] Tsung-Yi Lin, Priya Goyal, Ross Girshick, Kaiming He, and Piotr Dollár. Focal loss for dense object detection. In Proceedings of the IEEE international conference on computer vision, pages 2980–2988, 2017. 3

[21] Ze Liu, Yutong Lin, Yue Cao, Han Hu, Yixuan Wei, Zheng Zhang, et al. Swin transformer: Hierarchical vision transformer using shifted windows. In Proceedings of the IEEE/CVF international conference on computer vision, pages 10012–10022, 2021. 2, 3

[22] Natalie H Matthews, Wen-Qing Li, Abrar A Qureshi, Martin A Weinstock, and Eunyoung Cho. Epidemiology of melanoma. Exon Publications, pages 3–22, 2017. 1

[23] Piyu Parth Naik. Cutaneous malignant melanoma: A review of early diagnosis and management. World journal of oncology, 12(1):7, 2021. 1

[24] Jiquan Ngiam, Aditya Khosla, Mingyu Kim, Juhan Nam, Honglak Lee, and Andrew Y Ng. Multimodal deep learning. In Proceedings of the 28th international conference on machine learning (ICML-11), pages 689–696, 2011. 6

[25] Cristiano Patrício, João C Neves, and Luis F Teixeira. Coherent concept-based explanations in medical image and its application to skin lesion diagnosis. In Proceedings of the IEEE/CVF Conference on Computer Vision and Pattern Recognition, pages 3799–3808, 2023. 3

[26] Khoi Pham, Kushal Kafle, Zhe Lin, Zhihong Ding, Scott Cohen, Quan Tran, and Abhinav Shrivastava. Learning to predict visual attributes in the wild. In Proceedings of the IEEE/CVF conference on computer vision and pattern recognition, pages 13018–13028, 2021. 3

[27] MA Pizzichetta, R Talamini, I Stanganelli, P Puddu, R Bono, Giuseppe Argenziano, A Veronesi, GIUSTO Trevisan, H Rabinovitz, and H Peter Soyer. Amelanotic/hypomelanotic melanoma: clinical and dermoscopic features. British Journal of Dermatology, 150(6):1117–1124, 2004. 1

[28] Tal Ridnik, Emanuel Ben-Baruch, Nadav Zamir, Asaf Noy, Itamar Friedman, Matan Protter, and Lihi Zelnik-Manor. Asymmetric loss for multi-label classification. In Proceedings of the IEEE/CVF international conference on computer vision, pages 82–91, 2021. 3

[29] Olga Russakovsky, Jia Deng, Hao Su, Jonathan Krause, Sanjeev Satheesh, Sean Ma, et al. Imagenet large scale visual recognition challenge. International journal of computer vision, 115:211–252, 2015. 5

[30] Kalyan Saginala, Adam Barsouk, John Sukumar Aluru, Prashanth Rawla, and Alexander Barsouk. Epidemiology of melanoma. Medical sciences, 9(4):63, 2021. 1

[31] Rebecca L Siegel, Angela N Giaquinto, and Ahmedin Jemal. Cancer statistics, 2024. CA: A Cancer Journal for Clinicians, 2024. 1

[32] Peng Tang, Xintong Yan, Yang Nan, Shao Xiang, Sebastian Krammer, and Tobias Lasser. Fusionm4net: A multi-stage multi-modal learning algorithm for multi-label skin lesion classification. Medical Image Analysis, 76:102307, 2022. 1, 2, 3, 6, 7

[33] Adane Nega Tarekegn, Mario Giacobini, and Krzysztof Michalak. A review of methods for imbalanced multi-label classification. Pattern Recognition, 118:107965, 2021. 3

[34] Fiona M Walter, A Toby Prevost, Joana Vasconcelos, Per N Hall, Nigel P Burrows, Helen C Morris, et al. Using the 7-point checklist as a diagnostic aid for pigmented skin lesions in general practice: a diagnostic validation study. British Journal of General Practice, 63(610):e345–e353, 2013. 1

[35] Yuheng Wang, Jiayue Cai, Daniel C Louie, Z Jane Wang, and Tim K Lee. Incorporating clinical knowledge with constrained classifier chain into a multimodal deep network for melanoma detection. Computers in Biology and Medicine, 137:104812, 2021. 3

[36] Yan Wang, Yangqin Feng, Lei Zhang, Joey Tianyi Zhou, Yong Liu, et al. Adversarial multimodal fusion with attention mechanism for skin lesion classification using clinical and dermoscopic images. Medical Image Analysis, 81:102535, 2022. 1, 3, 6, 7

[37] Yongwei Wang, Yuheng Wang, Jiayue Cai, Tim K Lee, Chunyan Miao, and Z Jane Wang. Ssd-kd: A self-supervised diverse knowledge distillation method for lightweight skin lesion classification using dermoscopic images. Medical Image Analysis, 84:102693, 2023. 3

[38] Siyuan Yan, Zhen Yu, Xuelin Zhang, Dwarikanath Mahapatra, Shekhar S Chandra, Monika Janda, Peter Soyer, and Zongyuan Ge. Towards trustable skin cancer diagnosis via rewriting model's decision. In Proceedings of the IEEE/CVF Conference on Computer Vision and Pattern Recognition, pages 11568–11577, 2023. 7, 8

[39] Jordan Yap, William Yolland, and Philipp Tschandl. Multimodal skin lesion classification using deep learning. Experimental dermatology, 27(11):1261–1267, 2018. 6

[40] Yilan Zhang, Fengying Xie, and Jianqi Chen. Tformer: A throughout fusion transformer for multi-modal skin lesion diagnosis. Computers in Biology and Medicine, 157:106712, 2023. 1, 2, 3, 4, 6, 7